*R*esearch in
*A*stronomy and
*A*strophysics

An active coronagraph using a liquid crystal array for exoplanet imaging: principle and testing *

Xi Zhang[1,2,4], De-Qing Ren[1,2,3], Yong-Tian Zhu[1,2] and Jiang-Pei Dou[1,2]

[1] National Astronomical Observatories / Nanjing Institute of Astronomical Optics & Technology, Chinese Academy of Sciences, Nanjing 210042, China; *xzhang@niaot.ac.cn*

[2] Key Laboratory of Astronomical Optics & Technology, National Astronomical Observatories / Nanjing Institute of Astronomical Optics & Technology, Chinese Academy of Sciences, Nanjing 210042, China

[3] Physics & Astronomy Department, California State University Northridge, 18111 Nordhoff Street, Northridge, California 91330-8268, USA

[4] Graduate University of Chinese Academy of Sciences, Beijing 100049, China

Abstract High-contrast imaging coronagraphs, used for the detection of exoplanets, have always adopted passive coronagraph optical components. It is therefore impossible to actively optimize the coronagraphs to achieve their best performance. To solve this problem, we propose a novel high-contrast imaging coronagraph which combines a liquid crystal array (LCA) for active pupil apodization and a deformable mirror (DM) for phase correction. The LCA we use is an amplitude-only spatial light modulator. The LCA is well calibrated and compensates for its amplitude non-uniformity and nonlinear intensity responsivity. We measured the imaging contrasts of the coronagraph system with the LCA only and without the DM deployed. Imaging contrasts of 10^{-4} and 10^{-5} can be reached at an inner working angular distance of 2.5 and $5\lambda/D$, respectively. A simulation shows that the phase errors on the coronagraph pupil limit the contrast performance. The contrast could be further improved if a DM is deployed to correct the phase errors induced by the LCA and coronagraph optics.

Key words: instrumentation: coronagraph, liquid crystal array — techniques: high-contrast imaging, exoplanet detection

1 INTRODUCTION

Today, exoplanet detection is one of the most important topics in astronomy. More than 500 exoplanets have been identified as of 2011, and most of them were discovered by indirect approaches such as radial velocity detection. Since the discovery of the planets around the star HR 8799 in recent

years (Marois et al. 2008; Serabyn et al. 2010), the techniques for the direct imaging of exoplanets have attracted much attention. To image young and Jupiter-like planets, or even Earth-like planets, the diffraction lights from the observed central stars should be suppressed by high-contrast coronagraphs. For young and Jupiter-like planets, a contrast of 10^{-5} is required in the infrared, and the requirement increases to $10^{-9} \sim 10^{-10}$ for detecting Earth-like planets in the visible. The transmission pupil apodizing coronagraph is one example of a promising high-contrast coronagraph, in which the starlight on the pupil is modulated according to a designed function.

We proposed a stepped transmission filter-based coronagraph which is constructed by metallic coating techniques (Ren & Zhu 2007; Ren et al. 2010). Such a coronagraph system has been built in the laboratory and demonstrated its ability to deliver a contrast of 10^{-7} at an angular distance down to $5\lambda/D$ (Dou et al. 2010). However, the performance of this coronagraph is highly dependent on the manufacturing qualities of the transmission filters, i.e. the transmission precision.

Since in practice the transmission through each step of the metallic coating filters is fixed after being manufactured, the transmission errors can only be measured but not corrected, which seriously limits the coronagraph's performance. Here we propose a novel coronagraph that integrates an active liquid crystal array (LCA) and a deformable mirror (DM) to replace the conventional coronagraphs which only use passive optical components (Ren & Zhu 2011). In this approach, the LCA is used as a spatial light modulator (SLM) to actively control or correct the light transmission until the best coronagraph performance is achieved.

Another method to achieve flexible amplitude correction is to use the two-DM configuration (Roggemann & Lee 1998), which is applied for correcting the intensity variation induced by the turbulent atmosphere. This approach can only correct the amplitude distribution in a small range, and is not suitable for coronagraph pupil apodization, where a large transmission range from $\sim 0\%$ to $\sim 100\%$ is required. In our configuration of the proposed coronagraph, the LCA with voltages applied on its pixels is responsible for both active pupil apodization and transmission amplitude correction. Since each modulated LCA pixel with its voltage applied induces a corresponding phase change, variation of the voltage will induce a phase error.

As a result, the imaging contrast will be degraded. To solve this problem, a DM can be used to correct all the phase errors that are induced by the LCA and the coronagraph's optics.

In this paper, we present the principle of the active LCA coronagraph and its optical test configuration in Section 2. LCA calibration and amplitude correction, which are critical in reaching better high-contrast imaging performance, are also discussed in this section. In Section 3 we report our latest tests in the laboratory: the measured contrasts of 10^{-5} can be reached by the coronagraph with LCA only. We indicate that the phase correction through a DM can further improve the contrast in small inner working angular distances. Finally, we present our conclusions.

2 PRINCIPLES OF THE ACTIVE CORONAGRAPH AND AMPLITUDE CORRECTION

2.1 Amplitude Modulation of the LCA

A liquid crystal array is based on the birefringence of its nematic liquid crystal molecules. These cigar-shaped molecules are uniaxial crystals whose optical axes are parallel to the direction of the molecules. The long axis of the molecules defines the direction of the extraordinary index. Since the extraordinary index can change along with the voltages applied to the liquid crystal, the polarization orientation of the light transmitted will rotate for specific angles. Sandwiched between a polarizer and an analyzer, the LCA acts like an SLM. For the twisted nematic (TN) and vertical aligned nematic (VAN) reflective LCAs in common use, the main difference is the arrangements of their liquid crystal molecules: the molecules of TN LCAs rotate gradually in a helical fashion; by contrast, the molecules of VAN LCAs have no rotation. However, these two types of reflective LCAs can be

described by the same Jones matrix, written as follows (Lu & Saleh 1991; Yang & Lu 1999),

$$
J = \exp(-j2\beta)
\begin{pmatrix}
\left(\dfrac{\alpha}{\gamma}\right)^2 + \left(\dfrac{\beta}{\gamma}\right)^2 \cos 2\gamma - j\dfrac{\beta}{\gamma}\sin 2\gamma & -\dfrac{j\alpha(1-\cos 2\gamma)}{\gamma^2} \\[2ex]
-\dfrac{j\alpha(1-\cos 2\gamma)}{\gamma^2} & \left(\dfrac{\alpha}{\gamma}\right)^2 + \left(\dfrac{\beta}{\gamma}\right)^2 \cos 2\gamma + j\dfrac{\beta}{\gamma}\sin 2\gamma
\end{pmatrix},
\tag{1}
$$

where

$$
\gamma = \sqrt{\alpha^2 + \beta^2}\,,
\tag{2}
$$

$$
\beta = \frac{\pi d}{\lambda}(n_e - n_o)\,.
\tag{3}
$$

The angle α represents the twist angle of the top layer and bottom layer of the reflective LCA. n_o, n_e, λ and d are the ordinary and extraordinary indices of the liquid crystal material, the wavelength of the light transmitted and the depth of the liquid crystal layer, respectively.

In accordance with Equation (1), Lu and Saleh studied the characteristics of the reflective TN LCAs as amplitude modulators (Lu & Saleh 1991). Their conclusions can also be applied to the VAN LCAs. Assuming that the polarizer and the analyzer make the angles ψ_1 and ψ_2, respectively, with the long axis of the top layer liquid crystal molecules, the relative reflectance R and the phase error δ of an LCA (TN or VAN type) obey the following equations,

$$
R = \left\{\left[\left(\frac{\alpha}{\gamma}\right)^2 + \left(\frac{\beta}{\gamma}\right)^2 \cos 2\gamma\right]\cos(\psi_1 - \psi_2)\right\}^2
$$
$$
+ \left\{\frac{\alpha\beta}{\gamma^2}(1-\cos 2\gamma)\sin(\psi_1 + \psi_2) - \frac{\beta}{\gamma}\sin 2\gamma \cos(\psi_1 + \psi_2)\right\}^2\,,
\tag{4}
$$

and

$$
\delta = 2\beta + \tan^{-1}\left(\frac{\dfrac{\alpha\beta}{\gamma^2}(1-\cos 2\gamma)\sin(\psi_1 + \psi_2) - \dfrac{\beta}{\gamma}\sin 2\gamma \cos(\psi_1 + \psi_2)}{\left[\left(\dfrac{\alpha}{\gamma}\right)^2 + \left(\dfrac{\beta}{\gamma}\right)^2 \cos 2\gamma\right]\cos(\psi_1 - \psi_2)}\right)\,.
\tag{5}
$$

For a VAN LCA with the twist angle $\alpha = 0°$, the amplitude modulation is achieved by adjusting the polarizer angle $\psi_1 = 45°$, and the analyzer angle $\psi_2 = -45°$. The reflectance R and phase error δ in this case are written as

$$
R = \sin^2(2\beta)\,,
\tag{6}
$$

and

$$
\delta = 2\beta + n\pi, \qquad n = \pm 1, \pm 2, \dots\,.
\tag{7}
$$

Figure 1 shows the reflectance R and phase error δ as a function of β. The operational range of β for amplitude modulation is from 0 to 0.25π, which usually corresponds to an 8-bit range of applied voltages. For such a configuration, a minimum relative reflectance of 0 and maximum relative reflectance of 1 are reached at the two ends of the operational range of β, which means that the LCA can gradually modulate the output light from completely blocked to being freely passed. In addition, the phase error δ with a maximum value of 0.5π is linear in this range of β, which is an ideal condition for the follow-up phase corrections.
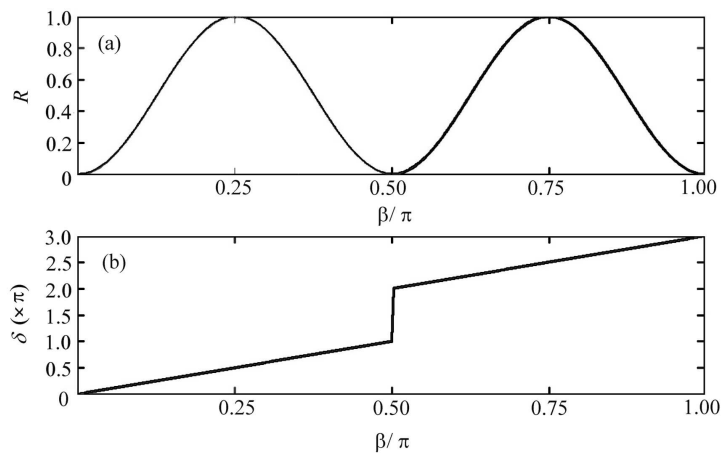
Fig. 1 Relative reflectance R as a function of β (a), and relative phase shift error δ as a function of β (b). The phase jump of δ occurs when R approaches 0.
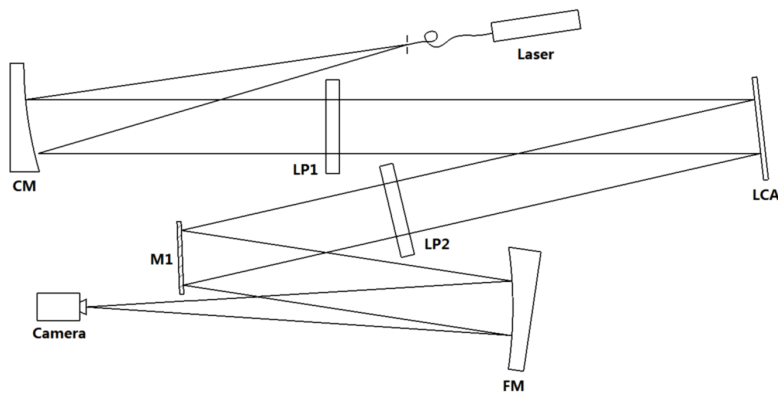
Fig. 2 The optical layout of the active LCA coronagraph: the light passes a collimating mirror (CM), a polarizer (LP1), an LCA, an analyzer (LP2), a folding mirror (M1) and a focusing mirror (FM) in sequence.

2.2 Conceptual Layout of an Active LCA Coronagraph

The optical layout of our active coronagraph with LCA is shown in Figure 2. The active coronagraph includes a collimating mirror, a polarizer, a reflective VAN LCA, an analyzer, a folding mirror and a focusing mirror. In laboratory tests, a laser light is fed into a single-mode fiber and the fiber's output end is placed at the focus of the collimating mirror to simulate the telescope focal plane's star light image. Currently, no actual DM is used in our coronagraph optics, since the effective phase correction requires a DM with a large number of actuators, which is very expensive. A DM with 24×24 actuators, a 3.5μm maximum stroke and 14-bit resolution is perfect for our application. Its dynamic phase range and phase precision are sufficient to correct the phase errors of a VAN LCA

that is estimated according to Equation (7). We plan to replace the folding mirror (M1 as shown in Fig. 2) with such a DM for real phase correction in our future works.

The LCA is connected to a control computer to create specific apodizing pupils. These pupil images are designed for different telescope systems and with specific contrast that is determined scientifically. The collimating light is reflected by the LCA that is sandwiched between the polarizer and the analyzer, and the intensity of the reflected light is modulated. High-contrast point spread functions (PSFs) are recorded by a scientific camera placed at the focal plane of the focusing mirror. After applying the initial apodizing pupil, the active coronagraph system should be further corrected for amplitude errors: the amplitude correction is done by the LCA itself, which adjusts the voltages applied on each pixel in closed loops according to a specifically optimized algorithm. In such a way, our coronagraph can be actively optimized for its best performance.

2.3 Amplitude Calibration and Correction for the LCA

To achieve the theoretical contrast, the amplitude distribution created by the LCA must be identical to the designed values. The nonlinear formula in Equation (6) indicates that there are large global amplitude errors on the actual apodizing pupil, compared with the designed pupil amplitudes. Moreover, the pixels on the LCA have an intrinsic non-uniform response towards amplitude modulation, which leads to the local amplitude errors. The defects in the optical components of the coronagraph's optics are also a factor that contributes both amplitude and phase errors. All of these amplitude errors will obviously change the amplitude distributions. Therefore, amplitude calibration and correction for the LCA is critical for achieving high-contrast imaging. Some papers have discussed LCA calibration and correction (Xun & Cohn 2004; Otón et al. 2007), but most of these discussions are based on the calibration and compensation for the LCAs as phase modulators. In these discussions, interferometers were used to calibrate phase errors: the amplitude non-uniformity of the LCA can only be partly compensated in such an indirect way. However, the amplitude errors induced by other optical components in the optics are still uncorrected, which calls for a direct approach to calibrate and correct the amplitude errors in each LCA pixel.

The ideal amplitude correction is to correct each single LCA pixel, however, this is difficult to achieve in real tests due to the inter-pixel coupling effect of the LCA pixels. We found that correcting a group of $N \times N$ LCA pixels as a whole, instead of correcting each single pixel, has the best correction results (here N is equal to five in our test). A group of $N \times N$ pixels covers a small continuous area on the LCA and is called point-like pixels herein. In this article, we propose an approach which directly calibrates and corrects the amplitude errors in a point-like pixel as shown in Figure 3(a), in which a point-like pixel corresponds to a small bright square spot. The actual recorded pupil image with an array of point-like pixels captured by a CCD camera is shown in Figure 3(b).

Since only the bright spots are recorded each time, and the dark areas around the spots cannot be recorded, the point-like pixel calibration is repeated by shifting the array image in the x and y directions in certain pixel distances by several steps, until all pixels on the LCA are recorded. By calculating the centroid of the spot images in Figure 3(b), the correspondences between the positions of these point-like pixels and their pupil images on the CCD camera are found. Assuming a point-like pixel of $N \times N$ LCA pixels has a theoretical coordinate of (x, y), the relative intensity of its reflected light $I_{lca}(x, y)$ is described as a function of the pixel intensity $I_{cam}(x', y')$ recorded by the camera,

$$I_{lca}(x, y) = \sum_{(x', y') \in D} I_{cam}(x', y') / \sum_{(x', y') \in D_{ref}} I_{cam}(x', y') , \qquad (8)$$

where D is the area defined by the centroid and average radius of the recorded point-like image on the CCD camera, and D_{ref} is the area of the reference point-like image. Assuming the theoretical relative intensity $I_t(x, y)$, we get the compensated relative intensity $I_{cmp}(x, y)$ of the point-like pixel (x, y) as described in Equation (9), and apply such intensity that is converted to an 8-bit gray scale
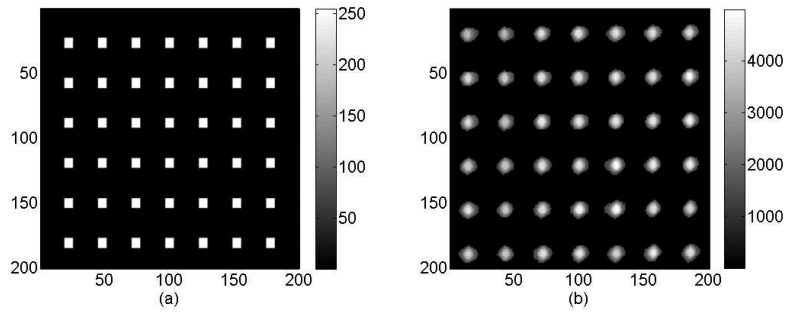
Fig. 3 An array of point-like pixels is sent to the LCA for calibration (a), and the pupil image is captured and processed for noise filtering (b). Each point-like pixel consists of 5×5 LCA pixels.
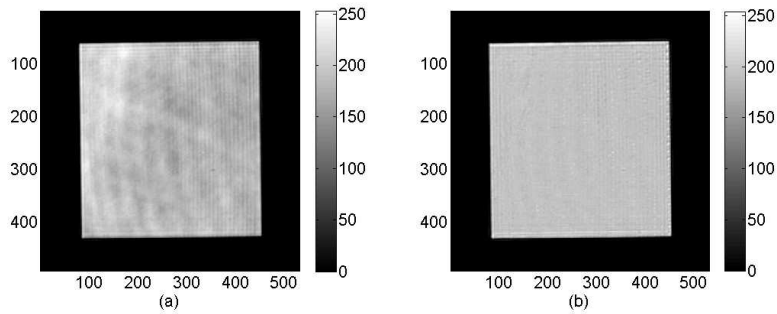
Fig. 4 The original pupil without amplitude correction (a), and the pupil after amplitude correction (b).

value on the LCA.

$$I_{\mathrm{cmp}}(x, y) = I_t(x, y)/I_{\mathrm{lca}}(x, y). \tag{9}$$

To ensure a good correction of amplitude errors, the algorithm is integrated into a closed loop that repeatedly measures $I_{\mathrm{lca}}(x, y)$, then calculates and updates $I_{\mathrm{cmp}}(x, y)$. In the real corrections, thresholds are adopted to limit the $I_{\mathrm{cmp}}(x, y)$ range in the closed loop to make the correction process smooth and convergent.

We demonstrate such a correction towards a square pupil with a size of 500×500 pixels that corresponds to 100×100 point-like pixels, in which each point-like pixel has 5×5 pixels. The square pupil is sent to the LCA with an identical gray scale value, without amplitude correction. In an ideal situation, the pupil image should be uniform. However, in reality the pupil is not uniform for the reasons discussed above, as shown in Figure 4(a). After amplitude correction, most of the amplitude errors in the LCA pupil have been corrected as shown in Figure 4(b): the RMS value of relative intensities drops from the original 8% to less than 1%. This algorithm is also effective for apodizing a pupil that contains multiple gray scale values. The related results will be shown in the next section.

3 TEST RESULTS

3.1 Contrast Test

The amplitude-modulation LCA that we used for the test is the LC-R 1080 from the HOLOEYE Company. This LCA has 8-bit electrical addressing and 1920×1200 pixels. A theoretical apodizing pupil with 50 rings, as shown in Figure 5(a), is optimized for an off-axis telescope without central obstruction. The apodizing pupil is designed to deliver contrast better than 10^{-5} at an angular distance $\geq 2\lambda/D$. Since the liquid crystal material has strong chromatic features, the transmission and phase are functions of wavelength. We have discussed the performance of the LCAs under different working wavelengths around the J band, and demonstrated that the chromatic aberration of the LCAs is sufficiently small to allow their use in ground-based telescopes in the near-infrared at a moderate contrast (Ren & Zhu 2011). Here, for the initial tests in the laboratory, a He-Ne laser with $0.633\,\mu m$ wavelength is used as the light source.

We still use 100×100 of the point-like pixels on the LCA to sample the 50-ring pupil image. The thresholds are set to 1% at the two ends of the intensity range, and the closed loop corrects up to 1% of the amplitude errors in each iteration. Good correction is achieved after 14 iterations, and the ring structures of the designed pupils, especially the outer dark rings, can be seen on the recorded pupil image as shown in Figure 6(b). As a result, the relative intensity difference between the actual

(a)   (b)
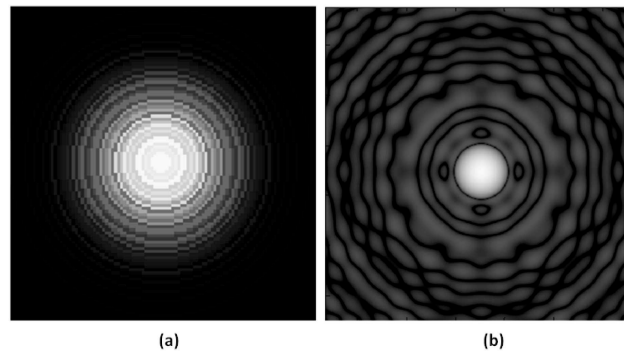
Fig. 5 The 50-ring apodizing pupil (a), and the associated PSF in log intensity scale (b).

(a)   (b)
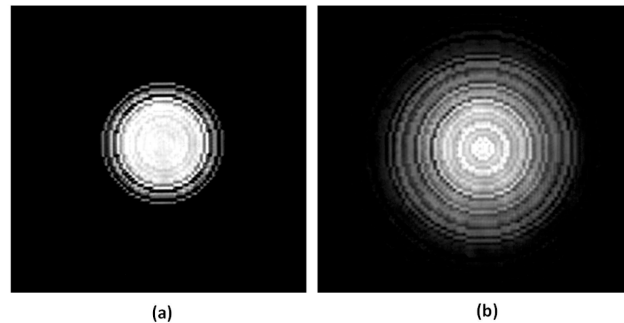
Fig. 6 Comparison between the actual measured pupil images before (a) and after (b) amplitude correction.
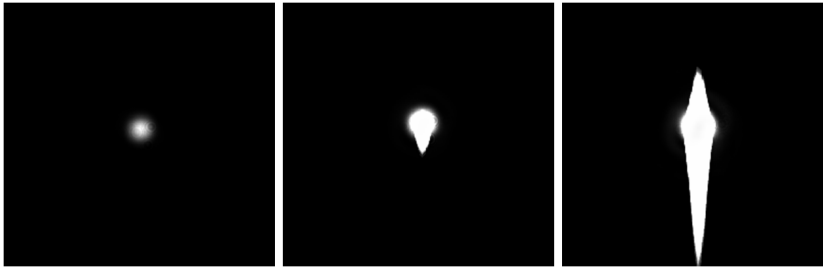
Fig. 7 The PSF images of the corrected pupil in different exposures. Exposure time increases from the left panel to the right panel. A 16-bit SBIG camera is used to take these images.

measured intensity pupil and the designed one, evaluated in terms of RMS value, is controlled below 7%, which compares with an initial RMS value larger than 18%.

The corrected pupil is used for the follow-up contrast test. The associated PSF images of the corrected pupil are recorded under three different exposures as shown in Figure 7. The average imaging contrasts are evaluated in six directions of these PSF images. Contrasts of 10^{-4} and 10^{-5} are achieved in the angular distance from $2.5\lambda/D$ to $12\lambda/D$, as shown in Figure 8. This contrast should be sufficient to detect the three outer planets around HR 8799 in the infrared on a 4 meter class telescope with a good adaptive optics system. Comparing with the designed contrast, the measured contrast outside $5\lambda/D$ is flat and close to the designed value of $10^{-5.5}$. However, there is still a larger difference in the range between $2.5\lambda/D$ and $5\lambda/D$, which is due to both the residual amplitude errors and the uncorrected phase errors.

3.2 Simulation for Phase Correction

Since there is no actual DM in the current optical system, a simulation is conducted instead of real phase correction to evaluate the influence of the phase error, which always accompanies the amplitude modulation of an LCA as described in Equation (7). Because the actual measured contrast profile is disturbed by measurement errors introduced by the CCD camera and other components in the coronagraph's optics, we use the simulated contrast profiles with and without phase correction for comparison, which can better reveal the effect of phase correction. In the simulation, the actual measured pupil intensity as shown in Figure 6(b) is used to calculate the phase errors according to Equation (7) in the range 0 to 0.5π. The actual measured pupil intensity is converted to its pupil amplitude and processed by a Fourier transform to simulate the PSF with phase correction. The pupil amplitude is then added with the calculated phase errors and also processed by a Fourier transform to simulate the PSF without phase correction. The simulation results are shown in Figure 9: the simulated contrast profiles without phase correction basically fit the actual measured contrast profile as drawn in Figure 8; meanwhile the phase errors degrade the contrast by three times on average by comparing the simulated contrast profiles with and without phase corrections. This indicates that the imaging contrast can be further improved by deploying a DM for phase correction. Here the stochastic parallel gradient descent (SPGD) algorithm is suitable for our application. It is based on the steepest descent optimization, and directly evaluates the PSF images according to a specific metric function. Combined with the SPGD algorithm, the DM is able to provide an extra contrast improvement of 30 times on average (Dong et al. 2011). We have also developed an iterative wave-front sensing algorithm that can directly measure large static wave-front errors from only one focal plane image (Dou et al. 2010). To further improve the contrasts in a specific area on the PSF images, both of the two algorithms can be used to correct the phase errors.

There are still differences between the simulated contrast with phase correction and the theoretical contrast, as shown in Figures 8 and 9, respectively, which means that the amplitude errors on the pupil still remain. This is due to the current 8-bit LCA lacking enough dynamic range to create a pupil that closely matches the theoretical values, which calls for new LCAs with a larger dynamic range to be used as amplitude modulators.
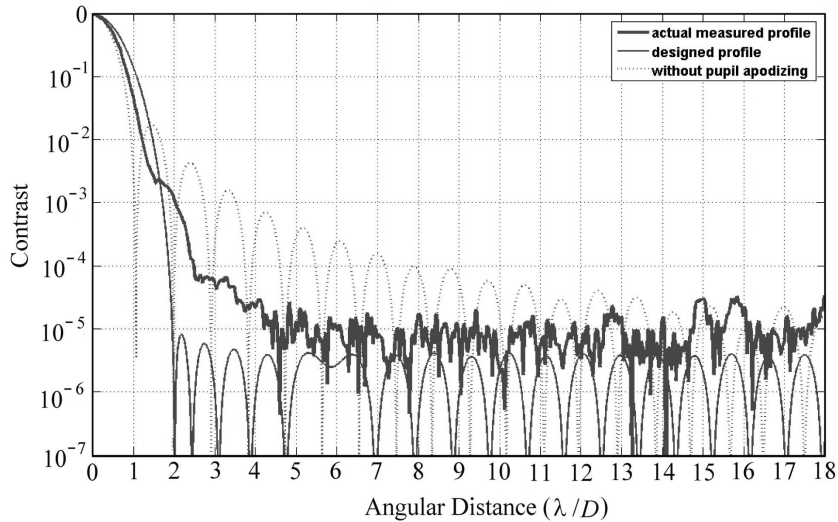
Fig. 8 Measured contrast after the amplitude correction: 10^{-5} contrast is achieved for an angular distance larger than $5\lambda/D$.
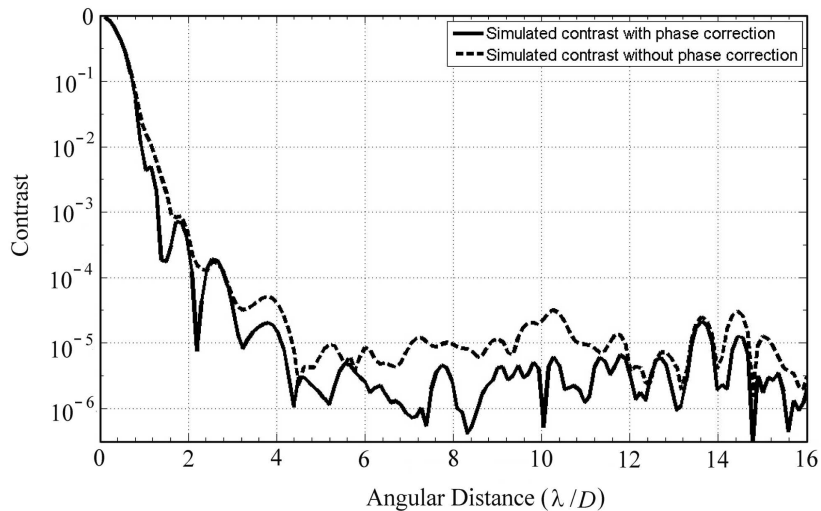
Fig. 9 Simulated contrast profiles for the cases with and without phase correction.

4 CONCLUSIONS

We proposed an active coronagraph based on an LCA and a DM for high-contrast imaging. The initial goal of this coronagraph system is to image young and Jupiter-like planets. The VAN LCA is chosen for modulating the amplitude of the coronagraph, which induces relatively small phase errors. We developed a compensation approach to correct the amplitude non-uniformity and other static amplitude errors in the coronagraph optics. For a designed 50-ring apodizing pupil, we corrected its amplitude distribution from the RMS values of 18% to 7%. An imaging contrast of 10^{-5} down to $5\lambda/D$ has been achieved in our laboratory tests after the amplitude correction, which is close to the designed contrast goal of $10^{-5.5}$. We further simulated the influence of the phase errors, which can be corrected by using a DM. The simulation indicates that high-contrast can be achieved at an angular distance down to $\sim 2\lambda/D$. Any further progress will be discussed in our future articles.

References

Dong, B., Ren, D.-Q., & Zhang, X. 2011, RAA (Research in Astronomy and Astrophysics), 11, 997

Dou, J.-P., Ren, D.-Q., & Zhu, Y.-T. 2010, RAA (Research in Astronomy and Astrophysics), 10, 189

Lu, K., & Saleh, B. E. A. 1991, Appl. Opt., 30, 2354

Marois, C., Macintosh, B., Barman, T., et al. 2008, Science, 322, 1348

Otón, J., Ambs, P., Millán, M. S., & Pérez-Cabré, E. 2007, Appl. Opt., 46, 5667

Ren, D., Dou, J., & Zhu, Y. 2010, PASP, 122, 590

Ren, D., & Zhu, Y. 2007, PASP, 119, 1063

Ren, D., & Zhu, Y. 2011, PASP, 123, 341

Roggemann, M. C., & Lee, D. J. 1998, Appl. Opt., 37, 4577

Serabyn, E., Mawet, D., & Burruss, R. 2010, Nature, 464, 1018

Yang, K. H., & Lu, M. H. 1999, Displays, 20, 211, *http://dx.doi.org/10.1016/S0141-9382(99)00025-6*

Xun, X., & Cohn, R. W. 2004, Appl. Opt., 43, 6400